*Article*

# Study on the Hydration and Microstructure of B and B/Na Ion-Doped Natural Hydraulic Lime Composed with Silica Fume/Fly Ash

**Yanbo Zhang, Ze Liu \*** , **Jixiang Wang, Conghao Shao, Jiaxing Li and Dongmin Wang**

School of Chemical and Environmental Engineering, China University of Mining & Technology, Beijing 100083, China
* Correspondence: lzk1227@sina.com

**Abstract:** Natural hydraulic lime (NHL) has drawn much attention due to its environmentally friendly nature. The characteristics of both hydraulic and pneumatic components make it a potential substitute for Portland cement in surface decoration and ancient building restoration. In this study, both doping and mixing with supplementary cementitious materials were investigated. Two types of NHL3.5 were fabricated through calcination at 1200 °C with B and B/Na doping, respectively. It is noted that B ion doping is beneficial to the early compressive strength of the specimens, and B/Na doping is beneficial to the later compressive strength of the specimens. The observed outcome is that the compressive strengths of B and coupled B/Na doped NHL3.5 are higher than the blank sample due to the appearance of α'-C2S. Thereafter, the blank and doping NHL were incorporated with fly ash and silica fume. The incorporation of fly ash and silica fume could enhance the early and late hydration rate. Of the two, silica fume shows more pozzolanic effect in the early age. In the supplementary cementitious materials dosed group, pozzolanic dominates the hydration process.

**Keywords:** natural hydraulic lime; ion doping; supplementary cementitious materials; hydration mechanism

## 1. Introduction

Hydraulic lime (HL) [1], one of the most historic cementitious materials, has recently drawn wide attention in both the restoration of ancient buildings and relics and the field of architecture. Traced back to the ancient Roman and Greek periods, people used lime-based cementitious materials (LCMs) as the main building binder [2,3]. It was not until the appearance of Portland cement and its promotion in the 18th century that lime-based cementitious materials were phased out of history [4]. In recent years, with the development of the concept of "green building materials", LCMs have gradually regained the focus of researchers worldwide. Compared with the calcination temperature of 1250~1450 °C for cementitious materials, the calcination temperature of HL is lower, usually 800~1200 °C, which greatly reduces the carbon emission in the production process [5,6]. HL also absorbs $CO_2$ from the air during the hardening process, which further reduces energy consumption and carbon emissions. At the same time, the choice of raw materials for the preparation of hydraulic lime is wider: marl [7], chalk [8], ginger nut [6], even dolomite [9] and other low-grade silica-calcium minerals that cannot meet the calcination conditions of the cement industry can be used as the main raw materials for natural hydraulic lime (NHL), which enhances the comprehensive utilization of minerals. Additionally, due to the wide range of raw materials, NHL's production conditions and application methods can be adapted to local conditions and reduce transportation costs to a certain extent. In conclusion, NHL has great potential for application in the construction field of ancient building restoration [10] and surface decorative mortars [11], coatings, etc. However, there are some problems in the application of hydraulic lime, such as cracking and salt petering [12]. In the field of ancient

building restoration, the long early setting time and low mechanical strength of hydraulic lime also seriously restrict its practical application [13]. The key to solving these problems is to improve the hydration activity of NHL materials and to conduct more in-depth research on the hydration mechanism and the working performance mechanism.

The main components of NHL include the gaseous hard component calcium hydroxide ($Ca(OH)_2$) and the hydraulic component ($2CaO\text{-}SiO_2$, $C_2S$). As reported, there are five types of polymorphs in $C_2S$, named $\alpha$, $\alpha'H$, $\alpha'L$, $\beta$, and $\gamma$, respectively [14]. Where $\alpha$, $\alpha'H$, and $\alpha'L$ phase are considered with high hydraulic reactivity, the instability at room temperature strongly restricts its application [15]. With respect to $\beta$ phase, it is the main crystalline phase of $C_2S$ in cement clinker and commercial NHL [16]. At the same time, $\gamma$ phase is commonly considered the most stable polymorph and hardly shows hydraulic reactivity [17]. Doping with impurity ions is one of the methods commonly used to improve the hydraulic activity of $C_2S$. $Na^+$, $Fe^{3+}$, $K^+$, $Mg^{2+}$, and other minor ions can be doped onto the $C_2S$ crystal to replace $Ca^{2+}$ or $[SiO_4]^{4-}$, which hinders the transformation of $C_2S$ into a rhombohedral crystal system during the cooling process [18,19].

It is well known that supplementary cementitious materials (SCMs) have a wide range of applications in the cement and hydraulic lime industry [20]. According to BSEN459:1-2010, NHLs can be referred as HLs when SCMs are added. SCMs have the following advantages: (i) reduced clinker usage; (ii) improved workability of the binder; (iii) pozzolanic activity can improve the mechanical strength of the matrix, etc. [21,22]. The commonly used SCMs are blast furnace slag (BFS) [23], fly ash (FA) [24], silica fume (SF) [25], and metakaolin (MK) [26]. In recent decades, the development of composite cement properties and microstructures has been a high research priority.

In this study, the NHL containing highly active $\alpha$ and $\alpha'$-$C_2S$ was prepared by first mixing limestone and diatomite according to the calcium-silica component requirements of BSEN459:1-2010 [27] for NHL3.5, then doping with a small amount of stabilizer (B, B/Na ions), followed by calcination and digestion. Then the fabricated NHL was complexed with FA and SF in different proportions and prepared as pastes with a fixed w/c ratio of 0.55. The hydration mechanism, microstructural changes, and mechanical properties of HL-based cementitious materials under the composite effect of dynamic material of SCMs and ion doping were investigated. In this paper, ion doping and SCMs were used together, and the hydration reaction difference of C2S with different crystal forms was explored. The early hydration reaction speed of NHL was improved and the application of NHL was expanded.

## 2. Materials and Methods
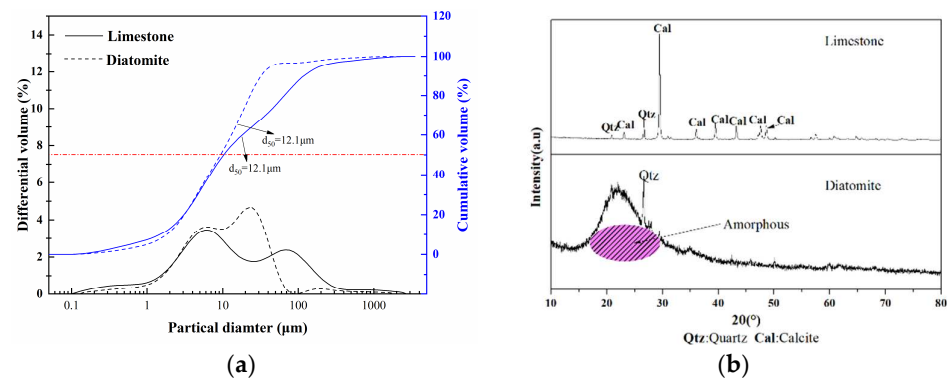
### 2.1. Materials

The NHL used in this study was fabricated in the laboratory. The raw materials used to prepare it are limestone from Liaoning Province and diatomite from Jilin Province, China. SCMs are fly ash and silica fume from Shanxi Province, China.

The chemical composition of raw materials is shown in Table 1. The raw materials were heated to 1000 °C to determine the loss on ignition (L.O.I) of raw materials, and the L.O.I of limestone at 1000 °C was 43.09 wt%, corresponding to a $CaCO_3$ content of about 97.9%. Meanwhile, the content of MgO is about 3 wt%, which, according to XRD results (Figure 1), mainly corresponds to dolomite ($CaMg(CO_3)_2$) in the raw material. According to the calculation, the Cementation Index (CI) value of the final product was 0.85 when adding 12% diatomite, which theoretically allows the production of natural hydraulic lime with high hydraulic properties.

$$CI = \frac{((2.8 \times \%SiO_2) + (1.1 \times \%Al_2O_3) + (0.7 \times \%Fe_2O_3))}{(\%CaO + 1.4 \times \%MgO)} \tag{1}$$

**Table 1.** Chemical components of the raw materials (wt%).

| Materials | CaO | SiO$_2$ | Al$_2$O$_3$ | Fe$_2$O$_3$ | MgO | SO$_3$ | Others | L.O.I |
|---|---|---|---|---|---|---|---|---|
| limestone | 48.33 | 3.61 | 0.81 | 0.73 | 3.00 | 0.05 | 0.38 | 43.09 |
| Diatomite | 0.32 | 86.20 | 2.03 | 1.93 | 0.26 | 0.29 | 0.82 | 8.14 |
| Fly ash | 2.88 | 50.54 | 26.86 | 5.95 | 0.74 | 0.52 | 5.93 | 6.59 |
| Silica fume | 0.18 | 92.70 | 0.14 | 0.04 | 0.64 | 0.59 | 0.84 | 4.87 |



(a)  (b)

**Figure 1.** (**a**) Particle size diameter distribution of raw material, (**b**) XRD patterns of the raw materials.

In this experiment, fly ash (FA) and silica fume (SF) were used as SCMs, where FA is mainly composed of CaO, Al$_2$O$_3$, Fe$_2$O$_3$, and other oxides. The content of CaO in FA is about 2.88%, indicating that it is low-calcium silicon FA. SF is acknowledged as highly reactive pozzolanic material, and its activity is mainly derived from the amorphous SiO$_2$, which accounts for 92.7% of the total content.

### 2.2. Preparation

According to the component requirements of BSEN459-1:2010 for NHL3.5, the Ca(OH)$_2$ content should not be less than 25%. Thus, the designed NHL3.5 consists of 75% C$_2$S and 25% Ca(OH)$_2$. First, 12 wt% diatomite was mixed with 88 wt% limestone as the calcined raw materials, added to 1.5 wt% B$_2$O$_3$, and 1.5 wt% B$_2$O$_3$ and Na$_2$CO$_3$ (in qual mass ratio) were mixed as stabilizers, respectively, and the mixture was ball-milled for 30 min until the particle size reached below 0.4 mm. As can be seen from Figure 2, the mixed powder was put into the muffle furnace, calcined at 1200 °C, with a heating rate of 5 °C/min and a holding time of 120 min. Then, 30% water by weight of the calcined product was weighed and mixed with the calcined product until the f-CaO was completely converted to Ca(OH)$_2$, which could be observed through the exothermic condition, and was dried at 80 °C after digestion for approximately 20 min. The final product was obtained after 30 min of grinding. The granularity of the final product reached 0.2 mm, the residual value of the sieve did not exceed 2% of the total mass of the sieved material, and the residual value of the sieve of 0.09 mm did not exceed 15% of the total mass of the sieved material.

Referring to the cement net test methods GBT1346-2011, 500 g of prepared NHL were added into the net paste mixer, water was added at a water-binder ratio of 0.55, the mixer was started and mixed at low speed for 120 s and then stopped for 15 s, and the slurry on the blade and pot wall was scraped into the pot and mixed at high speed for 120 s. It was poured into a 30 × 30 × 30 mm mold for molding. The molding temperature was 20 °C and the humidity was 60%. After 48 h, the demolded specimens were placed in the same environment and continued to cure to specific ages. At specific ages, the mechanical properties of the specimens were determined. Meanwhile, the hydration process was terminated by grounding into powder and soaking in ethanol. Before microscopic characterization, the samples were dried in a vacuum oven at 65 °C for 24 h. The mixture ratio is shown in Table 2.
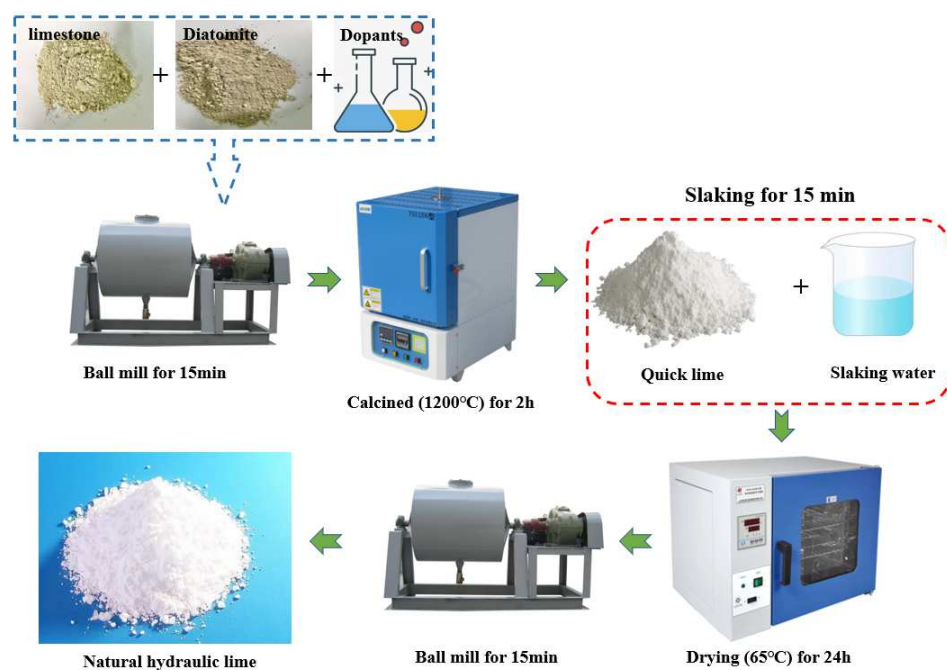
**Figure 2.** Schematic diagram of preparation process of natural hydraulic lime.

**Table 2.** Mixture mass (g) ratio of the materials in the experiment.

| | Sample | NHL | B1.5 | BNa1.5 | FA | SF |
|---|---|---|---|---|---|---|
| Blank | NHL | 500 | | | | |
| | F1 | 450 | | | 50 | |
| | F2 | 400 | | | 100 | |
| | S1 | 450 | | | | 50 |
| | S2 | 400 | | | | 100 |
| B-ion doping | B1.5 | | 500 | | | |
| | F1B1.5 | | 450 | | 50 | |
| | F2B1.5 | | 400 | | 100 | |
| | S1B1.5 | | 450 | | | 50 |
| | S2B1.5 | | 400 | | | 100 |
| B/Na doping | BNa1.5 | | | 500 | | |
| | F1BNa1.5 | | | 450 | 50 | |
| | F2BNa1.5 | | | 400 | 100 | |
| | S1BNa1.5 | | | 450 | | 50 |
| | S2BNa1.5 | | | 400 | | 100 |

### 2.3. Test Methods

The components of raw materials were measured by PANalytical Axios XRF (X-ray Fluorescence Spectrometer, PANalytical, Almelo, The Netherland). Smatlab X-ray diffraction (XRD, Rigaku Corporation, Tokyo, Japan) was used to determine the mineral composition of the raw material and specimens, with 40 kV and 40 mA, CuKa1 radiation. Furthermore, $10°/min$ and $1°/min$ increment and 1 s·step-1 sweep from $10°$ to $80°$ 2 h were adapted, respectively. Meanwhile, the Rietveld method was used for XRD data analysis to quantify the mineral phase content.

Tam Air 08 isothermal calorimeter (TA Instrument, New Castle, DE, USA), was used to determine the hydration heat of specimens. At 20 °C, the specimens were weighed and placed in 20 mL of ampoule according to the proportion, and water was added to them according to the W/B ratio of 0.55. They were stirred quickly and put into the calorimeter.

Fourier transform infrared spectroscopy (FT-IR) spectra were carried out in the range of $400–4000 \ cm^{-1}$ to determine chemical bonding and crystal structure changes. Microscopic

morphology and structure were determined by scanning electron microscope (SEM, Hitachi Regulus8100, Tokyo, Japan). The pore structure of the matrix is characterized by AutoPore IV 9500 Mercury intrusion porosimetry (MIP, Micromeritics Instrument, Norcross, GA, USA) in 30,000 psi. The mechanical properties of the specimens were measured on the same test machine (SANS CMT5105, Shenzhen, China) at a loading rate of $2400 \pm 200$ N/s.

## 3. Results

### 3.1. Mineral Content and Crystal Structure

For quantitative analysis, 20% rutile was mixed into the specimens as an internal calibrator. The XRD identified the five main mineral phases: portlandite, $\alpha'$-$C_2S$, $\beta$-$C_2S$, rutile (used as an internal standard), calcite, and magnesite, as shown in Table 3. The GSAS software was used to make a refined fit to the test data. The final fitting results are shown in Figure 3. The fit difference Rwp of each specimen is less than 10%, which indicates a good matching result. The main error is from $\alpha'$-$C_2S$ and $\beta$-$C_2S$, and the characteristic peaks of the two phases overlapped extensively.

According to the results of quantitative analysis, the content of magnesite is about 3.27~4.31%. It is in accordance with BS EN459-1 that the free MgO content of NHL should be less than 7%, and, after mixing with SCMs, the content of magnesite in the system will be further reduced. At the same time, Mg ions will participate in constituting other crystalline phases and amorphous phases in the system. The content of magnesite in all three types of NHL prepared in this experiment did not exceed the regulation, and magnesite did not affect the system significantly in the short term.

From Figure 3, it can be seen that in the undoped sample, the diffraction peaks of $C_2S$ are mainly $\beta$ phase, and in the B-doped sample there is an obvious crystalline transformation, and the diffraction peaks of $\alpha'$-$C_2S$ appear obviously at about $2\theta = 33°$. In addition, the diffraction peak at $2\theta = 33°$ tends to shift to a higher angle [28], which may be attributed to the replacement of small radius B ions with large radius Si ions in the doping process, and thus the size of $\alpha'$-$C_2S$ is reduced [29]. As can be seen from the composition of the specimens in Figure 3d, the content of $C_2S$ increases slightly after the incorporation of the stabilizer.

When B ions were doped, the $C_2S$ crystalline phase in the prepared NHL was $\alpha'$-phase with a content of 42.4 wt%, while 6.94 wt% of $\beta$-phase $C_2S$ was also present in the system, and when B/Na ions were doped, the content of $\alpha'$-$C_2S$ decreased to 38.56 wt%, whereas the content of the amorphous phase increased. This phenomenon is in agreement with the results of Chen, L. et al. [30]. Similarly, Álvarez-Pinazo et al. attributed this mainly to the presence of excess dopant in the belite as well as cell defects [31]. Additionally, the Na ions are said to have an antagonistic effect with B ions and stabilize more $C_2S$ into $\beta$ phase.

**Table 3.** ICCD-PDF and ICSD collection codes for all phases used for Rietveld refinements.

| Phase | Space Group | ICSD Code | PDF Code |
|---|---|---|---|
| $\alpha'$-$C_2S$ | Pnma | 81097 | 49-1674 |
| $\beta$-$C_2S$ | P121/N1 | 963 | 33-0302 |
| Portlandite | P-3M1 | 15471 | 44-1481 |
| Rutile | P42/mnm | 9161 | 21-1276 |
| Calcite | P3221 | 174 | 78-2315 |
| Periclase | Fm-3m | 9863 | 45-0946 |

In addition to their stabilizing effect on belite, B and Na ions are often used as mineralizing agents in the cement industry. Their addition can enhance the burnability of cement, lower the phase formation temperature of $C_2S$, $C_3S$, etc. [32,33], and improve the calcination effect. Therefore, after doping with minor ions, the denseness of calcination products rises and the crystal structure of CaO becomes more stable, which may affect its reaction with water and thus adversely affect its long-term stability [34]. It is inclined to be not easily pulverized during the digestion process, which is objectively manifested

by the rise in particle size of NHL, as shown in Figure 4. So the influence of doping ions can be concluded as doping B ion is more beneficial to the formation of $\alpha'$-C$_2$S, while doping B/Na ions lowered the content of $\alpha'$-C$_2$S. Mean, while B/Na ion doping shows more mineralization effect which led to the decrease in the content of portlandite and an increase in the particle size of the sample.
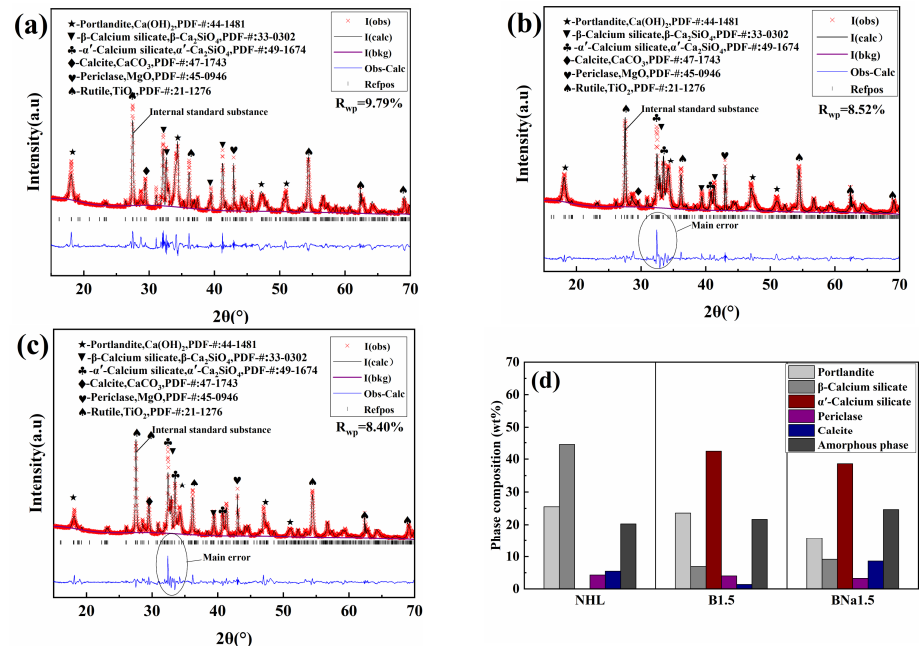


**Figure 3.** XRD fitting pattern of (**a**) NHL, (**b**) B1.5, and (**c**) BNa1.5; (**d**) mineral phase composition of the sample by Rietveld method.

It can be seen from Figure 5 that the characteristic bands near 842 cm$^{-1}$, 900 cm$^{-1}$, 1000 cm$^{-1}$ in the undoped samples correspond to the stretching vibrations of the Si-O bond and can be identified as $\beta$-C$_2$S [35]. Meanwhile, new bands near 746 cm$^{-1}$ and 1245 cm$^{-1}$ can be observed in the doped samples, corresponding to the bending and stretching vibrations of [BO$_3$]$^{3-}$. According to the research, the structure of $\alpha'$-C$_2$S stabilized by B ion can be defined as Ca$_{2-x}$B$_x$(SiO$_4$)$_{1-x}$(BO$_4$)$_x$, where the x is determined by the dosage of B ions as well as the ion types and quantity of raw material [36].
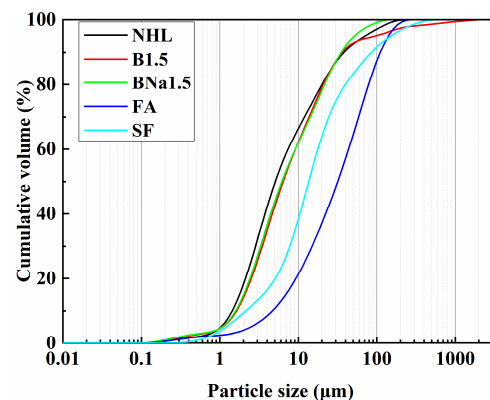


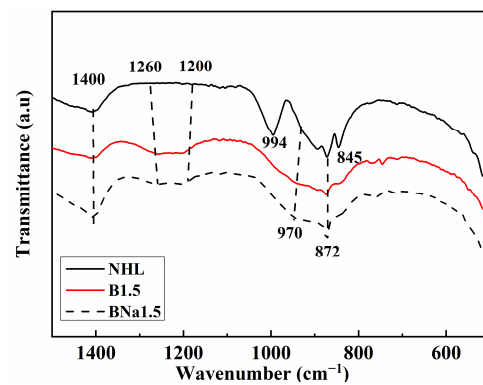**Figure 4.** NHL, FA, and SF particle size distribution.

**Figure 5.** FT-IR spectra of laboratory-prepared NHL.

Na$^+$ ion is considered an efficient dopant to stabilize β-C$_2$S. It is generally agreed that Na$^+$ ion can replace Ca$^{2+}$ in equivalent molar amounts in C$_2$S crystal [37]. For the samples with complex doping of B and Na ions, the characteristic spectra are similar to those of the single doped B ion specimens. Both [BO$_3$]$^{3-}$ as well as [BO$_4$]$^{5-}$ were present in the specimens. In the calcination process, due to the existence of different types of mineral phases, such as quartz phase, calcium oxide, calcite, etc., Na and B ions may occur in different degrees of solid solution with each mineral phase, which leads to the unequal doping of B and Na for C$_2$S [38].

The results of Rietveld refined cell parameters are shown in Table 4. The variation of the cell parameters of β-C$_2$S and α'-C$_2$S also shows that the cell volumes of β-C$_2$S and α'-C$_2$S appear to be reduced to different degrees in the single-doped specimens and the complex-doped specimens. The cell volume of β-C$_2$S is smaller in the single-doped specimens than in the complex-doped samples, while cell volume of α'-C$_2$S is smaller in the complex-doped samples. This is mainly due to the replacement of the large radius Si and Ca ions with the smaller radius B and Na ions. The different doping rates of B and Na atoms in β-C$_2$S and α'-C$_2$S cause different degrees of cell distortion. This result is also consistent with the FT-IR results.

**Table 4.** Lattice parameters of β-C2S and α'-C2S modified by the Rietveld method (Å).

| Samples | β-C$_2$S | | | | α'-C$_2$S | | | |
|---------|------|------|------|------|------|------|------|------|
|         | V | a | b | c | V | a | b | c |
| NHL | 345.74 | 5.51 | 6.76 | 9.32 | | | | |
| B1.5 | 337.96 | 5.50 | 6.64 | 9.27 | 345.08 | 6.84 | 5.46 | 9.25 |
| BNa1.5 | 345.68 | 5.51 | 6.75 | 9.31 | 344.91 | 6.85 | 5.45 | 9.24 |

### 3.2. Hydration Heat

The effect of doping and SCMs on the hydration characteristics of NHL was further investigated. Meanwhile, 10% and 20% FA and SF were added to the three types of NHL, respectively. Generally, the hydration process could be divided into four periods: (I) Initial reaction, (II) Inducing period, (III) Acceleration period, and (IV) Deceleration period. During the first period of mixed powder contact with water, the Ca(OH)$_2$ and C$_2$S dissolve and release a lot of heat [39]. Then the C$_2$S reacted with water and generated C-S-H gel layers which next act as a diffusion barrier coated with unreacted particles and restricted the hydration and pozzolanic reaction. Similar processes also occurred on the surface of SCMs particles [40]. Comparing the hydration exothermic curves of three specimens, NHL, B1.5, and BNa1.5, it is known that doping with B and Na ions significantly enhanced the hydration exothermic rate of the specimens. As can be seen from Figure 6, the exothermic rate curve of the blank group showed a continuous decay trend, and there was no obvious exothermic peak even till 160 h. Compared with the single doped B specimens, the exothermic peak of the coupled B and Na group appeared later, and its exothermic

peak appeared at about 120 h, followed by a slow decay, and the continuous exotherm still appeared at 220 h of hydration. This phenomenon is consistent with the strength development mode, which further indicates that the single-blended B has higher early strength, while the coupled B and Na have higher late strength.
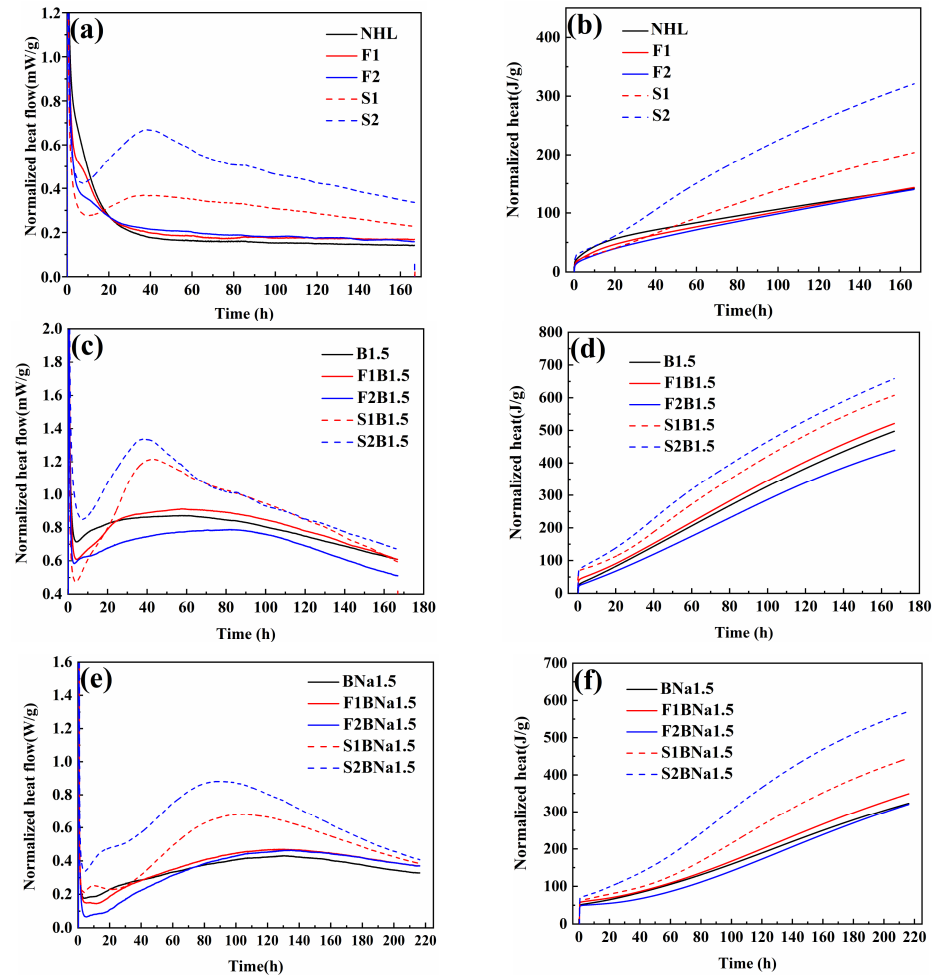


**Figure 6.** (**a**) Heat release rate curves of the blank group, (**b**) cumulative heat release of blank group; (**c**) heat release rate curves of B doping group; (**d**) cumulative heat release of B doping group; (**e**) the heat release rate curves of B/Na doping group; and (**f**) the cumulative heat release of B/Na doping group.

From Figure 6a, it can be seen that an obvious exothermic peak appeared at about 40 h after the incorporation of SF, and the peak intensity increased with the increase of SF mixing amount, which is due to the pozzolanic reaction of SF which generates a large amount of C-(A)-S-H gel and releases a large amount of heat. There is a slight decrease in the exothermic rate after the incorporation of fly ash, which indicates that FA is less involved in the early stage of hydration, while the relatively lower NHL content is another reason for the slower exotherm [41]. A similar phenomenon was also apparent in D. Zhang's study [42]. For the B-doped composite modified hydraulic lime, a significant increase in the hydration rate was observed for both specimens, relative to the blank group. As shown in Figure 6c, for the SF-doped specimens, an obvious exothermic peak appeared around 40 h, which can be identified as the exothermic peak generated by the pozzolanic reaction of SF after comparison with the blank group, which also indicates that the exotherm of pozzolanic reaction dominates the hydration in this stage. Thereafter, the exothermic curve gradually decreased, and at about 100 h, the curve of the SF-doped group was similar to the exothermic rate curve of the B1.5 specimen, indicating that the hydration of $C_2S$ dominated

at this stage and lasted until 160 h. In this group, the exothermic rate of the F1B1.5 specimen with 10% FA incorporation was higher than that of the B1.5 specimen (the exothermic rate curve became significantly steeper during the acceleration period), which may be attributed to: (i) The doping ions promoted the pozzolanic reaction of FA. (ii) The incorporation of FA increases the nucleation sites in the paste, which facilitates the nucleation growth of C-(A)-S-H gel. (iii) The "dilution effect" increases the contact between $C_2S$ and water, so it can fully engage in the hydration reaction, which also leads to the enhancement of the heat of hydration [43]. When 20% FA was added, the clinker and calcium hydroxide content in the system is further reduced, which caused a further decline in the exothermic rate. The pattern of the coupled B and Na doping group is similar to that of B doping single. In this group, the exothermic peak of SF-doped specimens appeared later at about 80 h. In general, SF promotes the early exotherm of the specimens due to the high pozzolanic activity, while the relatively early low pozzolanic activity of FA declined the hydration rate of the specimens. This is in agreement with the early mechanical strength.

### 3.3. Mechanical Properties

The pozzolanic reaction consumes a large amount of $Ca(OH)_2$ in the system, and the resulting C-(A)-S-H gel is similar to the hydration products of C2S. The decrease in alkalinity reduces the hydration rate of $C_2S$, but the C-(A)-S-H gel induces the hydration reaction of $C_2S$ in the long age, and the $Ca(OH)_2$ produced by the hydration reaction of $C_2S$ also promotes the secondary pozzolanic reaction of SCMs, so the incorporation of SCMs delays the hydration reaction of $C_2S$ in the early age, but promotes $C_2S$ reaction from two aspects in the long age.

It is noticeable that the doping significantly increased the compressive strength of the specimens. At the early stage of curing, the compressive strength of the B-doped specimens was higher, reaching 18 MPa at 21 d, which was 5 MPa higher than that of the coupled B/Na-doped specimens and much higher than that of the undoped specimens, which was 1.6 MPa. After 21 d, the strength growth of the B-doped specimens slowed down, while the strength of the coupled specimens accelerated, reaching 22.1 MPa at 60 d. The above results indicated that the B-doped specimens were more favorable to the early strength of the specimens, while the coupled B/Na was more favorable to the later strength of the NHL.

For the blank group experiments, the incorporation of SF significantly enhanced the early strength of NHL, as shown in Figure 7. In the high alkalinity environment, amorphous $SiO_2$ with high activity within SF can react with $Ca(OH)_2$ more quickly to form C-(A)-S-H gel; thus, the early strength of the mortar developed better. The strength of the specimen with 20% silica fume reached 14.8 MPa at 28 d. However, at the late stage of curing, the strength of the specimen showed significant inversion shrinkage and severe cracking at 60 d, making its strength untestable. This could be attributed to the quick early hydration of the specimen. During the hydration process, the free water in the pore decreases continuously with the reaction and produces partial minor shrinkage, while the hydration products bond the unhydrated particles into a shelf structure, and refill the cracks and pore structure, forming a relatively stable structure to resist part of the shrinkage stress [44]. Meanwhile, the curing condition is also one of the reasons for cracking. Some researchers use water curing or steam curing to reduce the water loss rate of cementitious materials, thus reducing the loss of structural water. At the same time, in the environment with high humidity, a small amount of calcium hydroxide will also dissolve in water and repair the possible micro cracks. The C-S-H gel is more evenly dispersed. This curing method is often used for the cementitious materials with high hydration speed to avoid cracks [45].
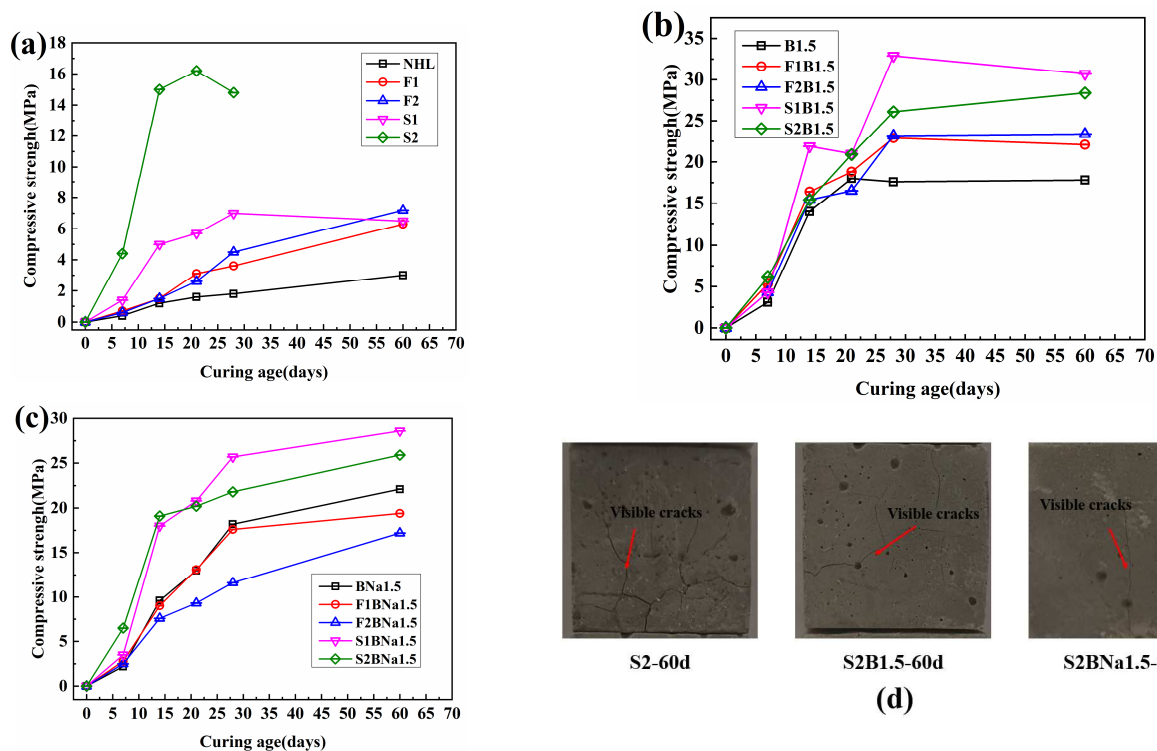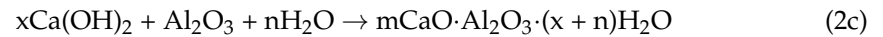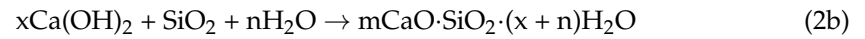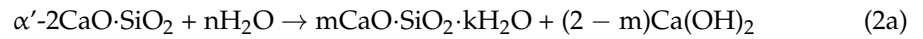
**Figure 7.** (**a**) Blank group, (**b**) B doping group, (**c**) B/Na doping group compressive strength, and (**d**) surface crack of the samples.

Due to the low early strength of NHL, it is not sufficient to resist the stresses due to shrinkage, thus producing cracks on the surface of the specimens, as shown in Figure 7d. The early strength of the FA-doped specimens in the blank group was lower compared to that of the specimens in the SF-doped group. The low early activity of FA is mainly related to its structure, which is a spherical particle covered with a glass layer that hinders the dissolution of the internal Si and Al phases. However, its strength is still slightly higher than that of the specimens without FA, which is mainly due to the interfiling of FA and lime particles, making the accumulation denser. In fact, at the initial stage, in addition to the degree of hydration, the filling effect and the surface properties of the particles also affect the strength of the specimens. The strength of the FA incorporated specimens continued to increase in the later stages of curing, as shown in Figure 7a. This is mainly due to the pozzolanic effect of FA of enhancing the strength of the specimens at the later stage [46]. In addition, the specimens in the FA dosed group were more structurally intact and did not show obvious cracks. On the one hand, the specimens in the early FA dosed group hydrated more slowly, thus the self-shrinkage was weaker and the shrinkage stress was low; on the other hand, the filling of FA between the particles optimized the structure of the specimens. In general, the SF-dosed specimens possessed higher early strength, but the mechanical properties deteriorated later due to self-shrinkage; the FA-dosed specimens had lower early strength but avoided microcracks in the specimens, and the pozzolanic effect of FA enhanced the mechanical properties of the specimens later. FA is considered to help reduce the cracking of cementitious materials.

After the doping of NHL, its composite modification with FA and SF resulted in some new effects on the specimens. First, for the specimens in the single B-doped group, the composite modification further improved the early mechanical properties of the specimens. The strengths of the specimens incorporated with 10% and 20% SF reached 32.9 MPa and 26.1 MPa at 28 d. The strengths of the specimens incorporated with 10% and 20% FA were 22.9 MPa and 23.2 MPa at 28 d, which were much higher than those of the blank group.

Two main types of hydration processes exist in this experiment. On the one hand, there is more $\alpha'$-$C_2S$ in the doped specimens, and its faster hydration rate at the early stage produces

part of the C-(A)-S-H gel; on the other hand, the dissolution and polymerization process of Si and Al phases in FA generates another part of C-(A)-S-H. These two processes together determine the strength of the composite modified specimens, as Equations (2a–c) show.

$$\alpha'\text{-}2CaO\cdot SiO_2 + nH_2O \rightarrow mCaO\cdot SiO_2\cdot kH_2O + (2 - m)Ca(OH)_2 \tag{2a}$$

$$xCa(OH)_2 + SiO_2 + nH_2O \rightarrow mCaO\cdot SiO_2\cdot(x + n)H_2O \tag{2b}$$

$$xCa(OH)_2 + Al_2O_3 + nH_2O \rightarrow mCaO\cdot Al_2O_3\cdot(x + n)H_2O \tag{2c}$$

These two hydration processes are not completely independent. In some previous studies, there are two main explanations for the interaction between the two processes. One explanation suggests that the promotion of alkalinity has a facilitated effect on the activity of fly ash [47]. The hydration process of the paste is accompanied by an increase in pH, and the increase in pH accelerates the erosion of the SCMs, thus more Si and Al phases are dissolved, which enhances the pozzolanic reaction. Another explanation is that the presence of SCMs has a facilitated effect on the hydration of $C_2S$ [48]. A.M. Sharar et al. [49]. suggested that $Ca(OH)_2$ covers the surface of $C_2S$ during hydration, which has a hindering effect on hydration. In contrast, the pozzolanic reaction consumes $Ca(OH)_2$, thus increasing the hydration activity of $C_2S$. It should be noted that both promotion mechanisms may exist simultaneously in the hydration process.

Finally, for the B-doped activation group, although some inversion of strength still occurred in the SF-doped specimens at the late stage of hydration, the inversion was improved relative to the blank group specimens, as can also be seen in Figure 7d, where the cracks on the surface of the S2B1.5 specimens were significantly reduced.

In general, SF with high volcanic ash activity can significantly promote the early hydration of NHL, while the effect of FA is not obvious at the early age and even reduces the early strength of NHL at 20% more incorporation. However, the effect of FA on the doped sample can significantly enhance the early performance of the matrix, owing to the interaction of the two hydration mechanisms. In addition, doping can avoid the inversion shrinkage problem caused by SF to some extent, which has a more positive effect on the mechanical properties of the binder.

### 3.4. Phase Analysis of Binders

As can be seen in Figure 8a, no significant change in the characteristic peak of β-$C_2S$ in the undoped NHL was observed due to the low early hydration activity of β-$C_2S$, and similar results were observed after the incorporation of FA. After the incorporation of SF, the characteristic peak of $Ca(OH)_2$ showed a significant decrease due to the high early pozzolanic activity and the characteristic peak of C-S-H gel was observed at 28 d, while the characteristic peak of β-$C_2S$ did not show significant changes.

For the specimens doped by single B, the characteristic peaks of $Ca(OH)_2$ in the non-SCMs-dosed and FA-dosed specimens increased with the curing time, while the characteristic peaks of $\alpha'$-$C_2S$ showed an obvious decline, and by 28 d the characteristic peaks of $\alpha'$-$C_2S$ showed an extremely weak "shoulder peak", as shown in Figure 8b. This indicates a faster hydration rate of $\alpha'$-$C_2S$ in ion-doped binder. It should be noted that the growth of $Ca(OH)_2$ can reflect the degree of hydration of the matrix to some extent, which is applicable to both cement and NHL systems, as demonstrated in many studies [50,51]. The FA-dosed specimen (F2B1.5) showed a more significant increase in $Ca(OH)_2$ characteristic peak intensity in 28 d compared with the un-doped specimen (B1.5), and this phenomenon supports the conclusion that FA has a facilitating effect on $\alpha'$-$C_2S$ hydration. The $Ca(OH)_2$ peak and $\alpha'$-$C_2S$ peak of SF-dosed specimens both weakened along the curing time, which proved that the pozzolanic effect had a greater influence on the hydration of the SF dosed specimens. The experimental phenomenon of the coupled B/Na doped group was similar to that of the single B doped group.
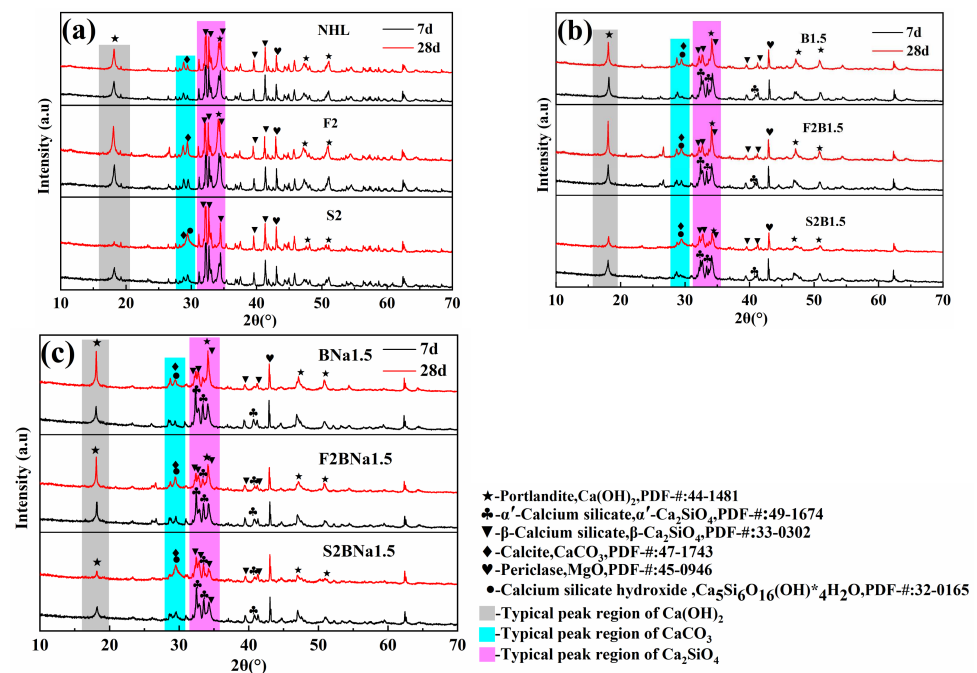
**Figure 8.** XRD of each sample curing for 7 d and 28 d: (**a**) blank series; (**b**) B-doped blank series; (**c**) B/Na-doped blank series.

### 3.5. TG Analysis

To further study the variation of the internal composition of the specimens with the degree of hydration, the variation law of chemically bound water and $Ca(OH)_2$ in the specimens at different ages was analyzed by TG. As can be seen from Figures 9 and 10 the weight loss of the specimen can be divided into four stages: −30–105 °C, 105–400 °C, 400–500 °C, and 500–800 °C. Where the weight loss below 105 °C is the evaporation of free water, 105–400 °C can be identified as C-(A)-S-H gel to remove chemically bound water, 400–500 °C is the dehydration of $Ca(OH)_2$, and 500–800 °C is the decomposition of $CaCO_3$ [52,53].
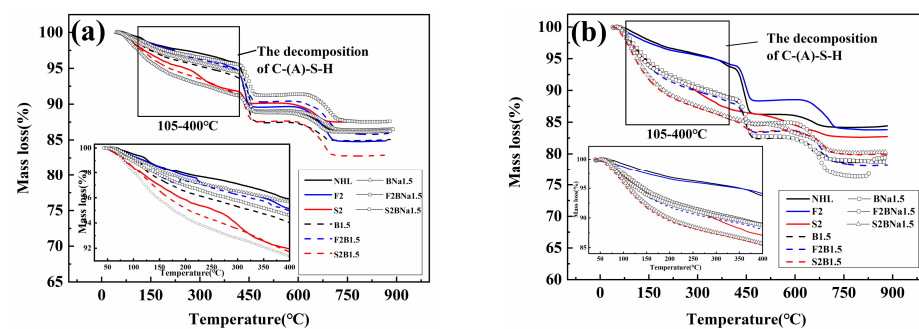


**Figure 9.** TG curves of the samples curing (**a**) 7 d; (**b**) 28 d.

The bound water content of all specimens increased with the extension of the curing time, and the bound water content of the doped specimens was higher than that of the blank group. At 7 d, the bound water content of single-doped B > coupled B/Na > blank group, while the strength of coupled B/Na was slightly higher than that of single-blended B at 28 d. This is consistent with the result that single-doped B specimens have higher early strength and coupled B/Na has higher late strength. This is consistent with the result that single-doped B has higher early strength and coupled B/Na has higher late strength. In the composite modified NHL coupled with SCMs, the binding water was partly derived from the hydration of $C_2S$ and partly from the pozzolanic reaction, and the FA, due to its

low activity and the substitution of clinker, led to a decrease in the binding water content after the FA incorporation, but in the doped group, the binding water of the FA specimens was significantly increased compared to the blank group, which again indicated that the doping had a facilitating effect on the pozzolanic activity. The higher pozzolanic activity of SF significantly enhanced the bound water in the specimens.
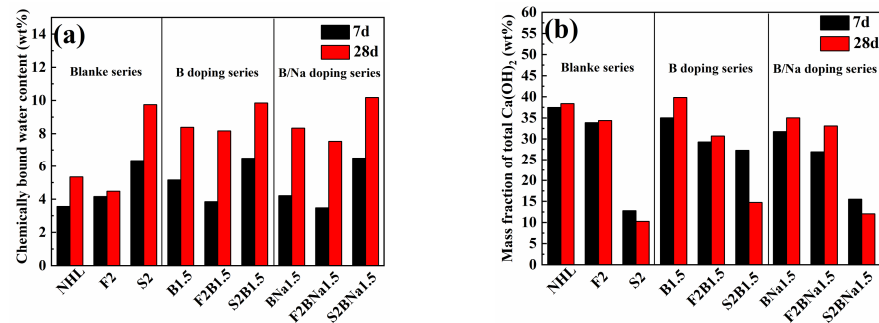


**Figure 10.** (**a**) Chemically bound water content of the samples at 7 d and 28 d; (**b**) total $Ca(OH)_2$ content in samples at 7 d and 28 d.

The variation of $Ca(OH)_2$ content then verifies the combined interaction of the two hydration mechanisms for the composite modified materials. For the doping samples only, the $Ca(OH)_2$ content increases with age, which corresponds to the hydration of $C_2S$, which reacts with water to produce $Ca(OH)_2$ in addition to the C-(A)-S-H gel. In contrast, for the composite modified system, the variation of $Ca(OH)_2$ content is the result of the competition between the two hydration mechanisms. For all SF-dosed samples, the $Ca(OH)_2$ content showed a decreasing trend with time, in which the $Ca(OH)_2$ content at 28 d: blank group < coupled B/Na doped < single-B doped group, which is due to the fact that the activated $SiO_2$ and $Al_2O_3$ would react with $Ca(OH)_2$ to form C-(A)-S-H gel. As for the doped specimens, the faster hydration of $\alpha'$-$C_2S$ to produce $Ca(OH)_2$ delayed the decrease of total $Ca(OH)_2$. The decrease in overall $Ca(OH)_2$ content then indicates that the strength of the pozzolanic reaction in the SF-doped composite modified NHL is greater than the hydration of $C_2S$. The $Ca(OH)_2$ content of FA-dosed composite modified NHL, on the other hand, increases slightly with the curing time, indicating that the hydration of $C_2S$ is stronger than the pozzolanic reaction during its hydration.

*3.6. Microstructure*

The microscopic morphology of 28 d specimens was analyzed by SEM as shown in Figure 11.

For the blank specimens without the addition of SCMs, the surface is dominated by a flocculent gel that grows on the surface of the particles. This flocculent gel structure is relatively loose, as shown in Figure 11a, and this type of gel is mainly generated at the early stage of hydration of $C_2S$. After ion doping, due to the higher degree of hydration, C-(A)-S-H grows and covers the surface of $C_2S$ particles, forming more widely distributed and dense gel, which is mainly needle-like with a mutual interweaving condition. The gel forms a "bridge" structure that connects particles to particles and supports the specimen, as shown in Figure 11b. For the specimens mixed with FA, two different types of gel were found. The surface of the FA particles is covered with a dense structured bulk gel, as shown in Figure 11c. Similar gel was found in Pengkun Hou's study on FA-Cement as a result of the pozzolanic reaction of FA [54]. The outside of this gel layer is covered with needle-like gel, which is generated due to the hydration of $C_2S$. For the SF-dosed specimens, the percentage of gel generated by the pozzolanic reaction is higher due to the higher pozzolanic activity of SF, as seen in Figure 11d, where the generated gel mainly appears plate-like. Furthermore, some petal-like gel was also found, and this gel was found to be similarly shaped in the morphological study by Xu, S. et al. [55] on the hydration products of NHL, which were

mainly generated by the hydration of $C_2S$, and the morphology of the gel was related to the water-ash ratio and the degree of hydration.
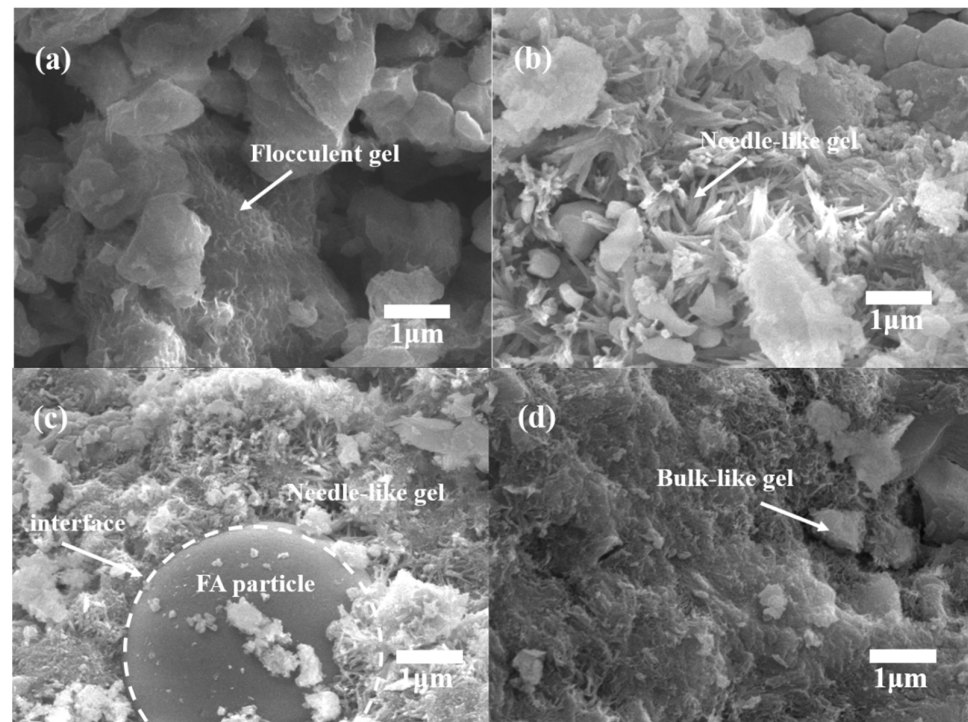


**Figure 11.** Micromorphology of samples at 28 d: (**a**) NHL, (**b**) B1.5, (**c**) F1B1.5, and (**d**) S2B1.5.

*3.7. Pore Structure*

The change of porosity of the specimen also reflects the different hydration degrees, and the pore size distribution of a typical specimens cured for 28 d is shown in Figure 12.
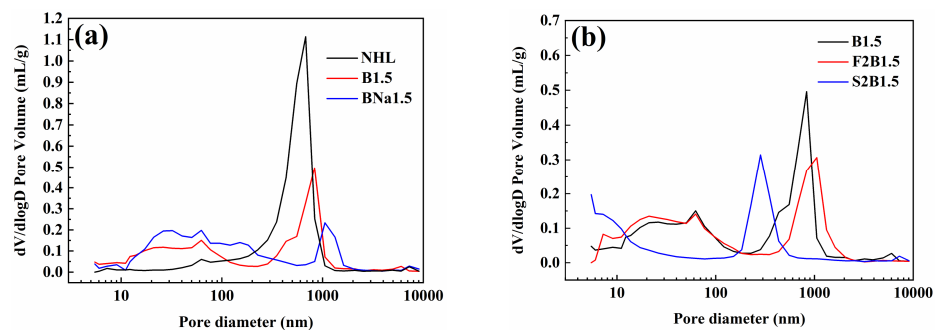


**Figure 12.** Pore structure distribution of typical samples cured for 28 d: (**a**) doped samples; (**b**) samples mixed with FA or SF.

The measured pores can be classified into four types according to their pore size: gel micropores (<4.5 nm); mesopores (4.5–50 nm); medium capillaries (50–100 nm); and large capillaries (>100 nm) [56]. From Figure 12a, it can be seen that the pore size of the blank NHL specimen is dominated by large capillary pores of about 700 nm, and the distribution of small pore size increases after doping, which shows that the number of large capillary pores larger than 100 nm decreases, while the number of medium-sized capillary pores within 0.01–0.1 μm increases, which indicates the increase of the dense degree of the doping matrix structure. The degree of denseness of the specimens can be judged according to the distribution of pore size: BNa1.5 > B1.5 > NHL, which is consistent with the law of compressive strength. After the addition of SCMs, there is a further reduction in the porosity of the matrix, as shown in Figure 12b. After the incorporation of FA, the

number of large capillary pores was reduced due to secondary hydration and filling, while the number of mesopores around 10 nm was increased. While the samples doped with SF showed a significant decrease in the large capillary pore size, mainly concentrated around 280 nm, the content of gel micropores and mesopores increased significantly, indicating that the structural denseness was significantly improved.

## 4. Conclusions

The effects of ion doping and SCMs on the mechanical strength of NHL were mainly investigated. The hydration rate, mineral phase evolution pattern, and microstructure of the material under the composite action were also investigated. On this basis, the hydration mechanism under the composite action was elaborated. The conclusions were obtained as follows:

Both single-doped B and couple-doped B/Na can stabilize $\alpha'$-$C_2S$, the stabilization effect of single-doped B on $\alpha'$-$C_2S$ is higher than that of couple-doped B/Na, and doping causes a decrease in the volume of $\alpha'$-$C_2S$ crystals. In addition, ion doping leads to the decrease of $Ca(OH)_2$ content in clinker and the increase of the amorphous phase, where the effect of complex B/Na doping is higher than that of single B doping.

Doping and the incorporation of FA and SF are able to enhance the mechanical strength of the specimens. The mechanical properties were further improved under the coupling effect. As far as doping is concerned, B doping is beneficial to the early strength of the specimens, and couple-B/Na doping is beneficial to the later strength of the specimens. After incorporation of SF, the high pozzolanic activity of SF significantly improved the early strength of the specimens, but the effect on undoped activated specimens leads to late cracking of the specimens and deterioration of the late strength. Doping can improve the degree of late cracking of the specimens. FA can effectively improve the late strength of the specimens, while for the doping group, FA incorporation specimens exhibit higher strength at an earlier period.

The composite modified lime strength is mainly related to the pozzolanic effect and $\alpha'$-$C_2S$ hydration. Doping significantly enhanced the hydration rate of the binder, with the single doped B group showing higher early hydration activity and the later hydration of the coupled B/Na, which was mainly dependent on the hydration of $\alpha'$-$C_2S$ in the specimens. The pozzolanic effect of SF is higher than the hydration of $\alpha'$-$C_2S$ in the couple-doped modification, while the pozzolanic reaction degree of FA is lower than the hydration of $\alpha'$-$C_2S$. The hydration of the matrix can be further promoted by the synergistic effect. Under the synergistic hydration, the gel in the material coexisted with the pozzolanic-generated gel and the $C_2S$-generated gel, and the gel generated by the pozzolanic effect is denser in structure, which reduces the porosity of the material.

**Author Contributions:** Conceptualization, Y.Z. and J.L.; methodology, J.W. and D.W.; data curation, Y.Z. and C.S.; writing—original draft preparation, Y.Z. and Z.L.; writing—review and editing, Y.Z. All authors have read and agreed to the published version of the manuscript.

**Data Availability Statement:** Not applicable.

**Conflicts of Interest:** The authors declare no conflict of interest.

## References

1. Arizzi, A.; Cultrone, G. Mortars and plasters—How to characterise hydraulic mortars. *Archaeol. Anthr. Sci.* **2021**, *13*, 144. [CrossRef]
2. Elsen, J.; Mertens, G.; Snellings, R. Portland Cement and Other Calcareous Hydraulic Binders: History, Production and Mineralogy. In *Advances in the Characterization of Industrial Minerals*; Mineralogical Society of Great Britian and Ireland: Twickenham, UK, 2011; pp. 441–479.
3. Artioli, G.; Secco, M.; Addis, A. *The Vitruvian Legacy: Mortars and Binders Before and After the Roman World*; Mineralogical Society of Great Britian and Ireland: Twickenham, UK, 2019; pp. 151–202.

4.  Hall, C. On the history of Portland cement after 150 years. *J. Chem. Educ.* **1976**, *53*, 222–223. [CrossRef]
5.  Han, T.H.; Ponduru, S.A.; Cook, R.; Huang, J.; Sant, G.; Kumar, A. A Deep Learning Approach to Design and Discover Sustainable Cementitious Binders: Strategies to Learn From Small Databases and Develop Closed-form Analytical Models. *Front. Mater.* **2022**, *8*, 574. [CrossRef]
6.  Jia, Q.Q.; Chen, W.W.; Tong, Y.M.; Guo, L.Q. Strength, hydration, and microstructure properties of calcined ginger nut and natural hydraulic lime based pastes for earthen plaster restoration. *Constr. Build. Mater.* **2022**, *323*, 126606. [CrossRef]
7.  Hughes, D.C.; Jaglin, D.; Kozlowski, R.; Mucha, D. Roman cements-Belite cements calcined at low temperature. *Cem. Concr. Res.* **2009**, *39*, 77–89. [CrossRef]
8.  Kalagri, A.; Miltiadou-Fezans, A.; Vintzileou, E. Design and evaluation of hydraulic lime grouts for the strengthening of stone masonry historic structures. *Mater. Struct.* **2010**, *43*, 1135–1146. [CrossRef]
9.  Yang, F.W.; Zhang, B.J.; Ma, Q.L. Study of Sticky Rice-Lime Mortar Technology for the Restoration of Historical Masonry Construction. *Acc. Chem. Res.* **2010**, *43*, 936–944. [CrossRef]
10. Ruegenberg, F.; Schidlowski, M.; Bader, T.; Diekamp, A. NHL-based mortars in restoration: Frost-thaw and salt resistance testing methods towards a field related application. *Case Stud. Constr. Mater.* **2021**, *14*, e00531. [CrossRef]
11. Bauerova, P.; Reiterman, P.; Davidova, V.; Vejmelkova, E.; Storkanova, M.K.; Keppert, M. Lime Mortars with Linseed Oil: Engineering Properties and Durability. *Rev. Romana Mater.* **2021**, *51*, 239–246.
12. Silva, B.A.P.; Pinto, A.P.F.; Gomes, A. Influence of natural hydraulic lime content on the properties of aerial lime-based mortars. *Constr. Build. Mater.* **2014**, *72*, 208–218. [CrossRef]
13. Maravelaki-Kalaitzaki, P.; Bakolas, A.; Karatasios, I.; Kilikoglou, V. Hydraulic lime mortars for the restoration of historic masonry in Crete. *Cem. Concr. Res.* **2005**, *35*, 1577–1586. [CrossRef]
14. Stankeviciute, M.; Siauciunas, R.; Miachai, A. Impact of $\alpha$-C2SH calcination temperature on the mineral composition and heat flow of the products. *J. Therm. Anal.* **2018**, *134*, 101–110. [CrossRef]
15. Wang, Q.; Manzano, H.; Guo, Y.; Lopez-Arbeloa, I.; Shen, X. Hydration Mechanism of Reactive and Passive Dicalcium Silicate Polymorphs from Molecular Simulations. *J. Phys. Chem. C* **2015**, *119*, 19869–19875. [CrossRef]
16. Morsli, K.; de la Torre, A.G.; Cuberos, A.J.M.; Zahir, M.; Aranda, M.A.G. Preparation and characterization of alkali-activated white belite cements. *Mater. Constr.* **2009**, *59*, 19–29.
17. Alonso, C.; Fernandez, L. Dehydration and rehydration processes of cement paste exposed to high temperature environments. *J. Mater. Sci.* **2004**, *39*, 3015–3024. [CrossRef]
18. Gawlicki, M. Effect of stabilizers on beta-C2S hydration. *Cem. Wapno Beton* **2008**, *13*, 147.
19. Huang, L.; Yang, Z. Sinterization and hydration of synthesized cement clinker doped with sulfates. *J. Therm. Anal.* **2019**, *138*, 973–981. [CrossRef]
20. Zhang, D.; Zhao, J.; Wang, D.; Xu, C.; Zhai, M.; Ma, X. Comparative study on the properties of three hydraulic lime mortar systems: Natural hydraulic lime mortar, cement-aerial lime-based mortar and slag-aerial lime-based mortar. *Constr. Build. Mater.* **2018**, *186*, 42–52. [CrossRef]
21. Uchima, J.S.; Restrepo-Baena, O.J.; Tobon, J.I. Mineralogical evolution of portland cement blended with metakaolin obtained in simultaneous calcination of kaolinitic clay and rice husk. *Constr. Build. Mater.* **2016**, *118*, 286–293. [CrossRef]
22. Wang, S.D.; Chen, C.; Gong, C.C.; Chen, Y.M.; Lu, L.C.; Cheng, X. Setting and hardening properties of alite-barium calcium sulfoaluminate cement with SCMs. *Adv. Cem. Res.* **2015**, *27*, 147–152.
23. Lin, K.-H.; Yang, C.-C. Effects of types and surface areas of activated materials on compressive strength of GGBS cement. *Mag. Concr. Res.* **2021**, *74*, 582–593. [CrossRef]
24. Cheng, Z.; An, J.; Li, F.; Lu, Y.; Li, S. Effect of fly ash cenospheres on properties of multi-walled carbon nanotubes and polyvinyl alcohol fibers reinforced geopolymer composites. *Ceram. Int.* **2022**, *48*, 18956–18971. [CrossRef]
25. Lu, D.; Shi, X.M.; Zhong, J. Interfacial nano-engineering by graphene oxide to enable better utilization of silica fume in cementitious composite. *J. Clean. Prod.* **2022**, *354*, 131381. [CrossRef]
26. Alelweet, O.; Pavia, S. Pozzolanic and hydraulic activity of bauxite for binder production. *J. Build. Eng.* **2022**, *51*, 104186. [CrossRef]
27. Grilo, J.; Faria, P.; Veiga, R.; Silva, A.S.; Silva, V.; Velosa, A. New natural hydraulic lime mortars–Physical and microstructural properties in different curing conditions. *Constr. Build. Mater.* **2014**, *54*, 378–384. [CrossRef]
28. Diouri, A.; Boukhari, A.; Aride, J.; Puertas, F.; Vazquez, T. Elaboration of alpha L'-C2S form of belite in phosphatic clinker. Study of hydraulic activity. *Mater. Constr.* **1998**, *48*, 23–32. [CrossRef]
29. Elhoweris, A.; Galan, I.; Glasser, F.P. Stabilisation of $\alpha'$ dicalcium silicate in calcium sulfoaluminate clinker. *Adv. Cem. Res.* **2020**, *32*, 112–124. [CrossRef]
30. Li, C.; Wu, M.X.; Yao, W. Effect of coupled B/Na and B/Ba doping on hydraulic properties of belite-ye'elimite-ferrite cement. *Constr. Build. Mater.* **2019**, *208*, 23–35. [CrossRef]
31. Álvarez-Pinazo, G.; Cuesta, A.; García-Maté, M.; Santacruz, I.; Losilla, E.; De la Torre, A.; León-Reina, L.; Aranda, M. Rietveld quantitative phase analysis of Yeelimite-containing cements. *Cem. Concr. Res.* **2012**, *42*, 960–971. [CrossRef]
32. Segata, M.; Marinoni, N.; Galimberti, M.; Marchi, M.; Cantaluppi, M.; Pavese, A.; De la Torre, G. The effects of MgO, $Na_2O$ and $SO_3$ on industrial clinkering process: Phase composition, polymorphism, microstructure and hydration, using a multidisciplinary approach. *Mater. Charact.* **2019**, *155*, 109809. [CrossRef]

33.  Fernandes, W.; Torres, S.; Kirk, C.; Leal, A.; Filho, M.L.; Diniz, D. Incorporation of minor constituents into Portland cement tricalcium silicate: Bond valence assessment of the alite M1 polymorph crystal structure using synchrotron XRPD data. *Cem. Concr. Res.* **2020**, *136*, 106125. [CrossRef]

34.  Abdelatif, Y.; Gaber, A.A.M.; Fouda, A.S.; Alsoukarry, T. Evaluation of Calcium Oxide Nanoparticles from Industrial Waste on the Performance of Hardened Cement Pastes: Physicochemical Study. *Processes* **2020**, *8*, 401. [CrossRef]

35.  Gualtieri, A.F.; Viani, A.; Montanari, C. Quantitative phase analysis of hydraulic limes using the Rietveld method. *Cem. Concr. Res.* **2006**, *36*, 401–406. [CrossRef]

36.  Cuesta, A.; Losilla, E.R.; Aranda, M.A.; Sanz, J.; De la Torre, G. Reactive belite stabilization mechanisms by boron-bearing dopants. *Cem. Concr. Res.* **2012**, *42*, 598–606. [CrossRef]

37.  Guo, P.; Wang, B.; Bauchy, M.; Sant, G. Misfit Stresses Caused by Atomic Size Mismatch: The Origin of Doping-Induced Destabilization of Dicalcium Silicate. *Cryst. Growth Des.* **2016**, *16*, 3124–3132. [CrossRef]

38.  Lai, G.C.; Nojiri, T.; Nakano, K. Studies of the Stability of Beta-$Ca_2SiO_4$ Doped by Minor Ions. *Cem. Concr. Res.* **1992**, *22*, 743–754. [CrossRef]

39.  Haustein, E.; Kuryłowicz-Cudowska, A.; Łuczkiewicz, A.; Fudala-Książek, S.; Cieślik, B.M. Influence of Cement Replacement with Sewage Sludge Ash (SSA) on the Heat of Hydration of Cement Mortar. *Materials* **2022**, *15*, 1547. [CrossRef]

40.  Wang, D.; Zhang, Q.; Feng, Y.; Chen, Q.; Xiao, C.; Li, H.; Xiang, Y.; Qi, C. Hydration and Mechanical Properties of Blended Cement with Copper Slag Pretreated by Thermochemical Modification. *Materials* **2022**, *15*, 3477. [CrossRef]

41.  Amin, M.S.; Abo-El-Enein, S.A.; Rahman, A.A.; Alfalous, K.A. Artificial pozzolanic cement pastes containing burnt clay with and without silica fume Physicochemical, microstructural and thermal characteristics. *J. Anal. Calorim.* **2012**, *107*, 1105–1115. [CrossRef]

42.  Zhang, D.; Zhao, J.; Wang, D.; Wang, Y.; Ma, X. Influence of pozzolanic materials on the properties of natural hydraulic lime based mortars. *Constr. Build. Mater.* **2020**, *244*, 118360. [CrossRef]

43.  Yoon, S.; Choi, W.; Jeon, C. Hydration properties of mixed cement containing ground-granulated blast-furnace slag and expansive admixture. *J. Mater. Cycles Waste Manag.* **2022**, *24*, 1878–1892. [CrossRef]

44.  Hasan, M.F.; Lateef, K.H. Effect of MK and SF on the concrete mechanical properties. *Mater. Today Proc.* **2021**, *42*, 2914–2919. [CrossRef]

45.  Kim, M.J.; Oh, T.; Yoo, D.Y. Influence of curing conditions on the mechanical performance of ultra-high-performance strain-hardening cementitious composites. *Arch. Civ. Mech. Eng.* **2021**, *21*, 104325. [CrossRef]

46.  Muthadhi, A.; Dhivya, V. Investigating Strength Properties of Geopolymer Concrete with Quarry Dust. *ACI Mater. J.* **2017**, *114*, 355–363. [CrossRef]

47.  Yang, L.; Zhao, P.; Liang, C.; Chen, M.; Niu, L.; Xu, J.; Sun, D.; Lu, L. Characterization and adaptability of layered double hydroxides in cement paste. *Appl. Clay Sci.* **2021**, *211*, 106197. [CrossRef]

48.  Poussardin, V.; Paris, M.; Tagnit-Hamou, A.; Deneele, D. Potential for calcination of a palygorskite-bearing argillaceous carbonate. *Appl. Clay Sci.* **2020**, *198*, 105846. [CrossRef]

49.  Sharara, A.; El-Didamony, H.; Ebied, E.; El-Aleem, A. Hydration characteristics of β-C2S in the presence of some pozzolanic materials. *Cem. Concr. Res.* **1994**, *24*, 966–974. [CrossRef]

50.  Lv, Y.J.; Yang, L.B.; Wang, J.L.; Zhan, B.J.; Xi, Z.M.; Qin, Y.M.; Liao, D. Performance of ultra-high-performance concrete incorporating municipal solid waste incineration fly ash. *Case Stud. Constr. Mater.* **2022**, *17*, e01155. [CrossRef]

51.  Rojo-Lopez, G.; Gonzalez-Fonteboa, B.; Martinez-Abella, F.; Gonzalez-Taboada, I. Rheology, durability, and mechanical performance of sustainable self-compacting concrete with metakaolin and limestone filler. *Case Stud. Constr. Mater.* **2022**, *17*, e01143. [CrossRef]

52.  Silva, A.S.; Cruz, T.; Paiva, M.J.; Candeias, A.; Adriano, P.; Schiavon, N.; Mirão, J.A.P. Mineralogical and chemical characterization of historical mortars from military fortifications in Lisbon harbour (Portugal). *Environ. Earth Sci.* **2011**, *63*, 1641–1650. [CrossRef]

53.  Ubbrìaco, P.; Traini, A.; Manigrassi, D. Characterization of FDR fly ash and brick/lime mixtures. *J. Therm. Anal.* **2008**, *92*, 301–305. [CrossRef]

54.  Li, P.; Ma, Z.; Li, X.; Lu, X.; Hou, P.; Du, P. Effect of Gypsum on Hydration and Hardening Properties of Alite Modified Calcium Sulfoaluminate Cement. *Materials* **2019**, *12*, 3131. [CrossRef] [PubMed]

55.  Xu, S.; Wang, J.; Sun, Y. Effect of water binder ratio on the early hydration of natural hydraulic lime. *Mater. Struct.* **2015**, *48*, 3431–3441. [CrossRef]

56.  Yang, Y.; Yan, Z.; Zheng, L.; Yang, S.; Su, W.; Li, B.; Ji, T. Interaction between composition and microstructure of cement paste and polymeric carbon nitride. *Constr. Build. Mater.* **2022**, *335*, 127464. [CrossRef]